Springer

KSME

Journal of Mechanical Science and Technology 28 (3) (2014) 867~877
www.springerlink.com/content/1738-494x
DOI 10.1007/s12206-013-1152-1

Aluminum 6060-T6 friction stir welded butt joints: fatigue resistance with different tools and feed rates †

S. Baragetti[1,2] and G. D'Urso[3,*]

[1]*Department of Engineering, University of Bergamo, Viale Marconi 5, 24044 Dalmine (BG), Italy*
[2]*Centre on Innovation Management and Technology Transfer, University of Bergamo, Via Salvecchio 19, 24129 Bergamo, Italy*
[3]*Department of Engineering, University of Bergamo, Viale Marconi 5, 24044 Dalmine (BG), Italy*

(Manuscript Received August 2, 2012; Revised June 28, 2013; Accepted September 27, 2013)

Abstract

The fatigue behavior of AA6060-T6 friction stir welded butt joints was investigated. The joints were produced by using both a standard and a threaded tri-flute cylindrical-tool with flat shoulder. The friction stir welding process was carried out using different feed rates. Preliminary tensile tests, micrograph analyses and hardness profile measurements across the welds were carried out. Welded and unwelded fatigue samples were tested under axial loading (R = 0.1) with upper limits of 10^4 and 10^5 cycles, using threaded and unthreaded (standard) tools at different feed rates. The best tensile and fatigue performance was obtained using the standard tool at low feed rate.

Keywords: Aluminum alloys; Friction stir welding; Joints microstructure; Static and Fatigue resistance

1. Introduction

Friction stir welding (FSW) is a solid-state welding process first introduced by TWI in Cambridge (UK) and patented in 1991 [1, 2]. This welding process is based on a rotating tool driven into the material and translated along the interface of two or more plates. Friction heats the material which is extruded around the tool and forged by the large pressure produced by the tool shoulder. FSW may offer several advantages: high quality joints, precise external control and high levels of repeatability, no need of special preparation of the samples, low energy process requirements and low creation of waste or pollution. The technology is also suitable for light weight alloys, particularly aluminum, that are often difficult or impossible to weld using conventional welding technologies (e.g., TIG or laser welding). In addition, friction stir welded joints are obtained through the deformation of the material at temperatures below the melting point, thus reducing problems related to distortions and residual stresses, if compared to traditional welding techniques.

So far, the FSW technique has successfully been applied to weld aluminum alloys in a number of applications such as automotive, aerospace, shipbuilding and railway [3]. This has justified the growing research efforts in shedding light on the microstructural aspects and the mechanical properties of FS-welded joints [3-5]. Compared to traditional fusion welding, FSW has shown excellent results in terms of structural strength in joining similar and even dissimilar aluminum alloys [3, 4] or Al-based particulate metal-matrix composites [6, 7]. The fatigue behavior analyses of FSW components have been extensively studied [3-15]; nevertheless further studies are needed before FSW can be safely used for high performance components. Process parameters such as feed rate, rotational speed, tool geometry [16-23] and residual stresses from FSW or post-process treatments [24-35] are critical factors, being strictly related to the mechanical properties of aluminum friction stir welded joints. Of particular interest is the effect of residual stresses on the fatigue crack propagation behavior of FSW joints [29-33]. Besides the experimental work, models accounting for the residual stresses have been developed to predict the fatigue crack growth through the welded material [34, 35].

Aluminum alloys in the 6xxx series can undergo suitable heat treatments to achieve attractive mechanical properties for a broad range of applications, including aircraft structures [36] and automotive skins [36, 37]. Their relatively high strength-to-mass ratio makes them profitable for meeting the pressing environmental concerns that prompt the automotive industry to reduce the weight of components. Thus, a wider use of FSW to join 6xxx aluminum sheets or plates could be very important. Significant research studies on the microstructure [38-40], crystallographic texture [41, 42], mechanical properties [7, 11-14, 18, 23, 39] and fatigue crack growth behavior

*Corresponding author. Tel.: +39 035 2052330, Fax.: +39 035 2052043
E-mail address: durso@unibg.it
† Recommended by Editor Jai Hak Park

[31, 43] of friction stir welded joints on alloys of this series have already been undertaken. However, to obtain a reliable understanding of the influence of the process parameters on the fatigue behavior of FSW joints, a larger amount of fatigue data on 6xxx alloys is needed. Up to now, the fatigue behavior of FSW butt joints of 6xxx alloys has been investigated mainly at fatigue lives longer than 10^4 load cycles [7, 12, 14, 23] and, in a few studies, also in the low cycle fatigue (LCF) regime [11, 13]. In Ref. [6], available fatigue data on FSW of aluminum alloys have been reviewed to derive a set of reference fatigue (S-N) curves through statistical analysis. The fatigue strength at $2 \cdot 10^6$ cycles and the slope k of the corresponding S-N curve for some alloys of the 6xxx series are provided. Kim et al. [11] performed fatigue tests on AA6005-T5 extruded aluminum alloy sheets welded with FSW and gas metal arc welding (GMAW). A sensitivity analysis of FSW performances was conducted by varying three design variables over two levels. The strength of the FSW joints was notably better than that of the GMAW ones and the fatigue resistance decreased with increasing the tool welding and rotating speed and with decreasing the tilt angle. A study of the fatigue behavior of FSW and metal inert gas (MIG) butt welds of 3 mm thick plates of AA6082-T6 and AA6061-T6 alloys was carried out by Moreira et al. [13]. The alloys were friction stir welded with tools of different dimensions using the same welding speed, tilt angle and tool rotating speed. The joints produced by MIG welding showed a higher decrease in the material mechanical properties than those prepared by FSW. Furthermore, the friction stir welded AA6061-T6 samples exhibited lower fatigue lives than the AA6082-T6 ones when tested at values of maximum stress (R = 0.1) lower than 130 MPa. In Ref. [22], Cirello et al. examined the influence of relevant FSW process parameters, the tool rotating speed, the feed rate and the tool sinking into the samples, on the fatigue resistance of AA6082-T6 butt joints. The variation of the process parameters had little influence on the fatigue resistance of the welded joints. The feed rate per unit revolution advancing ratio was the most relevant parameter in determining the mechanical strength of the joints. Feng et al. [10] observed the effects of the welding parameters on the LCF behavior and on the microstructure evolution of friction stir welded AA6061-T651 alloy. The rotational speed was found to have a negligible influence on the mechanical properties of the joints, whereas the fatigue life increased with the welding speed. FSW samples showed shorter fatigue lives, along with stronger cyclic hardening if compared with those of unwelded ones. The influence of FSW on the fatigue life of AA6063-T6 notched samples was investigated in Ref. [12]. A lower notch sensitivity of the welded alloy was pointed out. Attempts to predict the fatigue life of unwelded and welded samples in both the elastic and the plastic region of the strain-life curve were made.

As far as the authors know, the fatigue behavior of FSW joints of aluminum alloy AA6060 in the artificially aged condition T6 is still matter of debate. Furthermore, there is a lack of studies that compare between the fatigue performances of joints stirred with unthreaded and with threaded tools. Aissani et al. [16] observed that the use of a conical tri-flute threaded pin at very low feed rate allowed to produce AA2024-T4 and AA7075-T6 joints with good microstructures and microhardness properties. In Ref. [44], Lakshminarayanan et al. found superior tensile strength of AA6061 FSW joints in comparison with GMAW and GTAW joints of the same alloy. Threaded pins were used in Ref. [18] to apply the Taguchi based Grey relational analysis to optimize the tensile and elongation properties of friction stir welded AA1050-H22 aluminum alloy. In this work, AA6060-T6 friction stir welded butt joints were cycled under axial loading at R = 0.1 with upper limits of 10^4 and 10^5 repetitions. The fatigue strength of the base material under the same test conditions was also determined. The test samples were cut from groups of plates welded at different feed rates –150 or 600 mm/min – and by using either an unthreaded or a threaded tri-flute cylindrical-shouldered tool. Tensile tests and hardness measurements across the welds were also performed to gain a more comprehensive view of the effects of each welding condition on the mechanical properties of the joints. Cross-sectional macrographs were taken to identify the affected zones of the weld beads associated with the FSW processes and to highlight the changes amongst the different joints.

Table 1. Chemical composition of the base material (AA 6060-T6).

Component	wt.%
Aluminum, Al	<= 97.8 %
Chromium, Cr	<= 0.050 %
Copper, Cu	<= 0.10 %
Iron, Fe	0.10 - 0.30 %
Magnesium, Mg	0.35 - 0.60 %
Manganese, Mn	<= 0.10 %
Other, each	<= 0.050 %
Other, total	<= 0.15 %
Silicon, Si	0.30 - 0.60 %
Titanium, Ti	<= 0.10 %
Zinc, Zn	<= 0.15 %

2. Experimental technique

2.1 Friction stir welding

The experimental campaign was performed with a CNC machine tool. Butt joints were carried out on sheets having a thickness equal to 5 mm. An aluminum alloy AA6060 (Al-Mg-Si-Cu) in the artificially aged condition T6 was considered for this purpose. The chemical composition of the material is reported in Table 1.

Two different tools were used: a standard and a threaded tool. The first tool was a very simple device with a smooth flat shoulder and a cylindrical pin fabricated using AISI 1040 steel

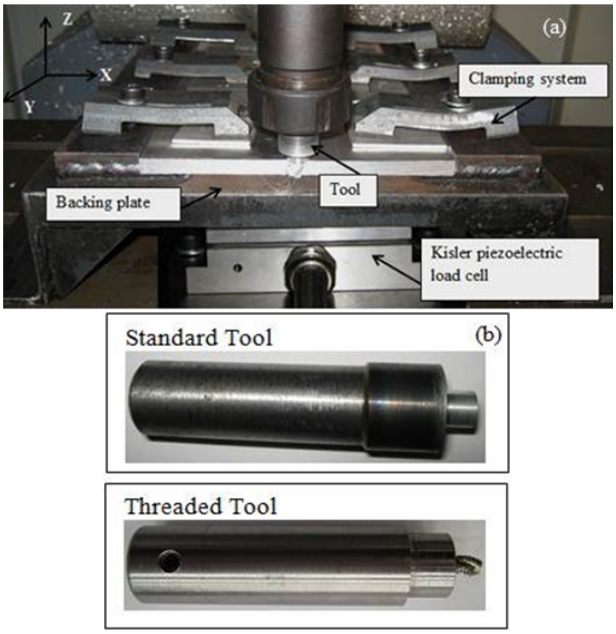

Fig. 1. A schematic diagram of the experimental setup: (a) experimental setup; (b) standard and threaded tools.

in the annealed condition; shoulder and pin diameters were, respectively, equal to 15 and 5 mm. The second one was a more complex tool based on two main components: a tool holder, with a flat shoulder, and a threaded probe obtained using a commercial M5 thread forming tap (Material: High Speed Steel - HSSE, coating: Br-R < 850 N/mm^2). Several welding operations were carried out by varying the process parameters, namely tool rotational speed (S = 2000 rpm) and feed rate (f = 150–600 mm/min). The same tilt angle, equal to 2.5°, was assumed for all the experiments. Fig. 1 shows the experimental setup and the tools.

2.2 Sample preparation

Samples for tensile tests with a minimum cross section of about 125 mm^2 (width equal to 25 mm) were obtained from the welded plates. The samples were prepared to investigate the mechanical properties of welded joints along a direction orthogonal to the welding path and assuming a tensile direction parallel to the rolling direction of the aluminum plates. Note that all the samples were extracted in the last part of the welded blanks, where steady state conditions can be assumed.

Smooth dogbone FS-welded and unwelded fatigue samples were also prepared. The welded ones were formed with the load axis transversal to the weld direction and with the weld bead in the middle of the gage length (Fig. 2). The work region was machined with a large radius of curvature of 40 mm, obtaining a K_t value less than 1.08, as confirmed by finite element analysis. Four series of welded samples were prepared according to the combinations of process parameters

Table 2. FSW fatigue samples: main process parameters.

Series ID	No. of samples	FSW process parameters		
		Feed rate (mm/min)	Rotational speed (rpm)	Tool shape
U-150	25	150	2000	Unthreaded
U-600	30	600	2000	Unthreaded
T-150	30	150	2000	Threaded
T-600	29	600	2000	Threaded
BM	30	-	-	-

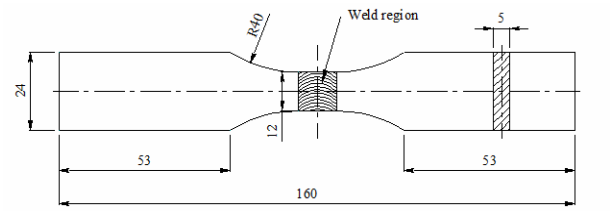

Fig. 2. Details of the FSW fatigue sample showing the nominal dimensions.

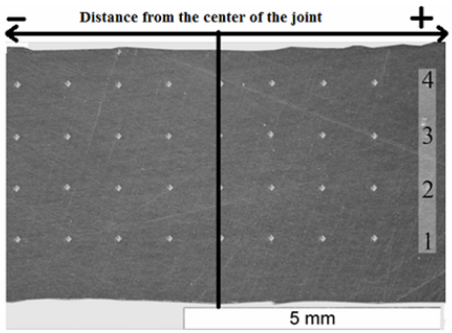

Fig. 3. Example of the Micro-Vickers indents distribution.

reported in Table 2. The number of samples available for each series is included in the same table. Unwelded samples (BM-samples) were tested under the same conditions of the welded ones for comparison (Table 2).

2.3 Mechanical and microstructure analyses

A universal Galdabini testing machine with a load cell of 50 kN was used to evaluate the mechanical properties of the FSW specimens. All tests were conducted under displacement control using a 0.5 kN preload and a speed of 5 mm/min.

Concerning hardness measurements, a sample was extracted from each welded plate by cutting it along the orthogonal direction with respect to the welding path. Micro-Vickers tests were carried out using a load of 5 N and 15 seconds of load time. In particular, a grid composed of four lines of indentations (moving from a distance of 1 mm to a distance of 4 mm from the upper surface) was executed on each sample. Every measurement campaign was composed of 144 (36 for each line) micro-Vickers tests, with a 1 mm gap between each indentation. Fig. 3 shows an example of the

Table 3. Loading ranges of the fatigue tests.

Upper limit (No. of cycles)	Loading range (MPa)				
	U-150	U-600	T-150	T-600	BM
10^4	142.5-152.5	142.5-150	122-152	112-137	200-250
10^5	140-150	130-145	122-137	77-97	190-230

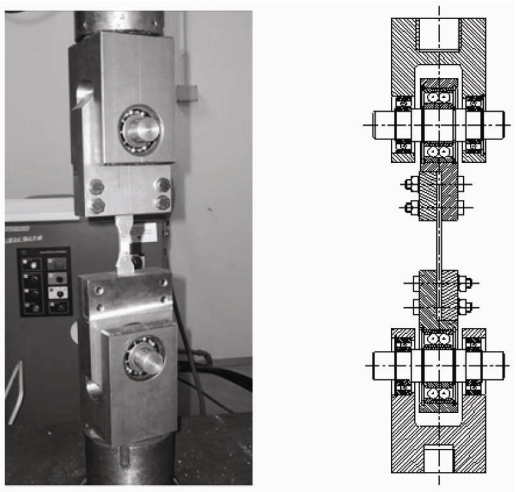

(a) (b)

Fig. 4. Fatigue testing system: (a) picture of the clamping system; (b) assembly drawing.

Micro-Vickers indents distribution. All the samples were analyzed with the advancing side on the left and the retreating side on the right.

A metallographic analysis was carried out to analyze the microstructure of the cross section of the joints as a function of the process parameters, and to evaluate the grain size in the different regions of the welded area. An electrolytic etching was performed in the following conditions: Barker's reagent, voltage = 20 V DC, current density = 0.2 A/cm^2, permanence time = 4 min. The etching procedure adopted for this analysis was derived from a common practice protocol, while the etching time was optimized for the specific case.

2.4 Fatigue tests

The fatigue samples were cycled under tension-tension (R = 0.1) loading using a computer-controlled universal testing machine (Instron 1273) at a frequency of 2 Hz in laboratory air at room temperature. Each series of samples was divided into two halves of fifteen samples, each of which was tested with an upper limit of 10^4 or 10^5 load cycles (Table 3). The staircase method [45-48] was implemented to determine the average value of fatigue limit, and all the experimental data were treated according to the statistical analysis procedure reported in ASTM E 739–91 [49]. The fatigue samples were loaded using the ranges reported in Table 3, by applying constant load increments between 2.5 and 5 MPa.

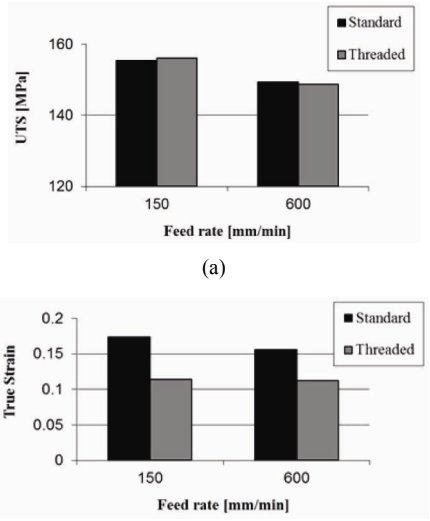

Fig. 5. Mechanical properties of the joints as a function of the process parameters: (a) UTS; (b) true strain.

Special grips (Fig. 4(a)) were used to prevent any parasite bending moment. Fig. 4(b) shows a cross-sectional view of the sample grip assembly, where several ball bearings (two of which can support quite high angular misalignments) were used to release the rotational degrees of freedom of the grips, hence creating two pin connections at the grip areas of the specimen.

3. Results and discussion

3.1 Evaluation of the tensile properties

The mechanical properties of the base material were: UTS = 251.8 MPa, Yield strength = 222.9 MPa. The main results in terms of UTS and true strain, as a function of feed rate and rotational speed for both threaded and standard tools, are reported in Fig. 5. Each histogram represents the average of five tests.

Rupture was normally localized in the heat affected zone (HAZ) on the retreating side. With respect to the base material, good results in terms of tensile strength and corresponding strain were found for both the tool geometries. Regardless of the tool shape, the best UTS (156 MPa) was obtained with a feed rate equal to 150 mm/min, corresponding to a welding efficiency of 62%. The welding efficiency resulting from the tensile tests is congruent with the values recommended by the standards for other traditional welding techniques (e.g., 0.6 for full penetration welds AA6060 T5 or T6 – UNI 8634-1985). Nevertheless, in FSW the post-process treatments are a significant factor, being strictly related to the mechanical properties, and aluminum alloys in the 6xxx series can undergo suitable heat treatments to achieve attractive mechanical properties for a broad range of industrial applications. Feed rate resulted to be the most significant

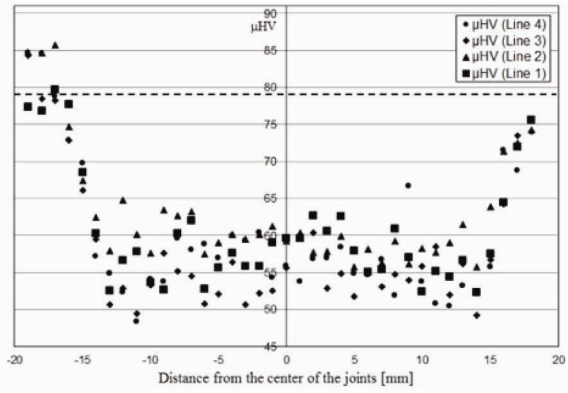

(a)

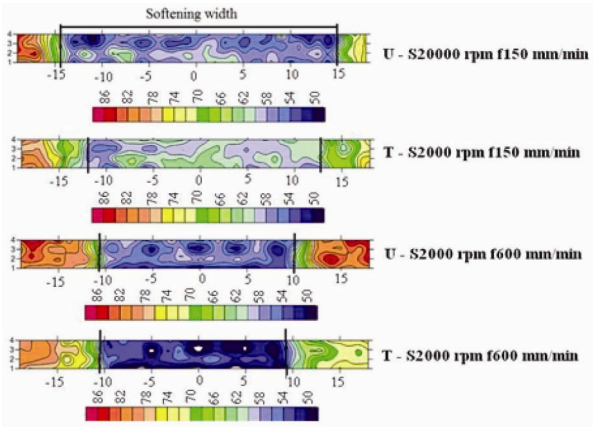

(b)

Fig. 6. Microhardnes properties of the joints: (a) typical microhardness distribution measured on the joint section (S = 2000 rpm, f = 150 mm/min); (b) graphical plot of microhardness distribution observed for different welding conditions.

parameter affecting the UTS. Tool geometry did not influence the UTS, while it played a fundamental role in determining the strain at rupture, the threaded tool being detrimental to the strain limit.

3.2 Microhardness and macrostructure

The typical microhardness distribution obtained on the joint section is reported in Fig. 6(a). As it is possible to notice, the hardness in the welded region is significantly lower with respect to that of the base material (79 μHV, represented by the horizontal dashed line). The width of the softened region and the microhardness values recorded in the same area resulted to be influenced by the welding process parameters.

In particular, the width of the softened area increases with decreasing values of feed rate. Fig. 6(b) shows the graphical plot of microhardness distribution at the different feed rates (150 and 600 mm/min) and for both the tool geometries.

The micrograph pictures regarding the electrolytic etching are shown in Fig. 7 (S2000 f150 (a) threaded and (b) unthreaded tool) and Fig. 8 (S2000 f600 (a) threaded and (b)

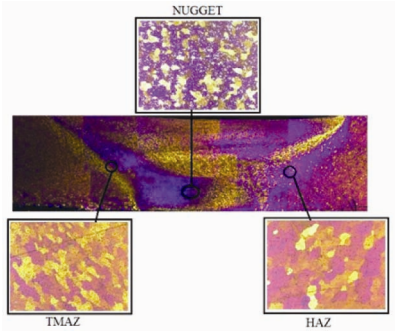

(a)

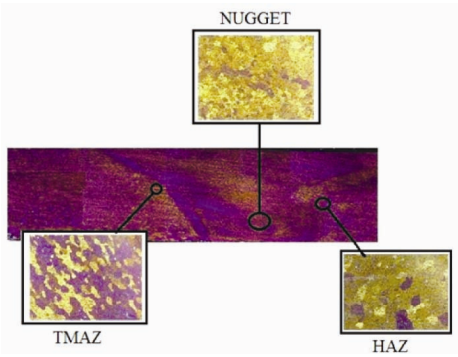

(b)

Fig. 7. Micrograph details: (a) S2000 f150 threaded tool; (b) S2000 f150 unthreaded tool.

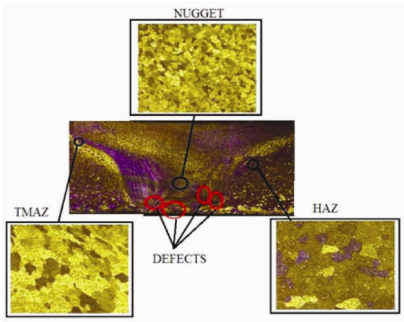

(a)

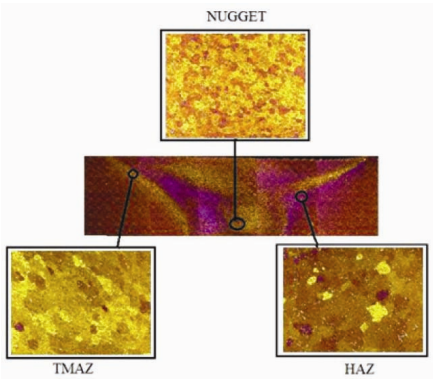

(b)

Fig. 8. Micrograph details: (a) S2000 f600 threaded tool; (b) S2000 f600 unthreaded tool.

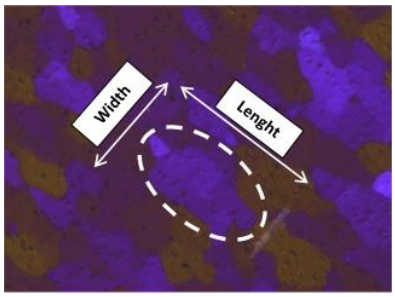

Fig. 9. Dimensions (length and width) of a representative grain.

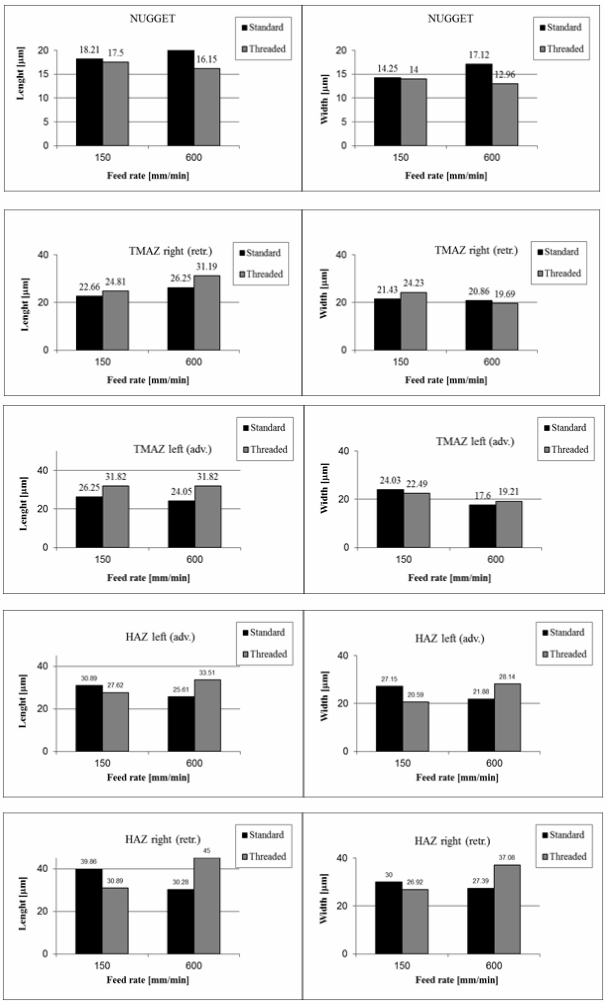

Fig. 10. Grain size (µm) in the welding regions as a function of the process parameters.

unthreaded tool).

A standard method for the grain counting, defined in Ref. [50], was applied on all the samples, and the grain size was evaluated within all the representative regions of the joint: nugget, thermomechanical affected zone (TMAZ), HAZ. Concerning HAZ and TMAZ, both the advancing and the retreating sides were taken into account. The grain size was evaluated in terms of both length and width of the grains, as shown in Fig. 9. The results of the analysis are reported in Fig. 10.

As a general remark, the average grain size in the nugget area is always smaller when the threaded tool is used. Considering the HAZ, the average grain size of the retreating side, where the failure occurred, is usually larger than the advancing one.

This is a qualitative consideration since the grain counting method takes into account a representative number of grains but not the entire amount of grains of each investigated region. In the other regions no systematic behavior is exhibited by varying the welding conditions.

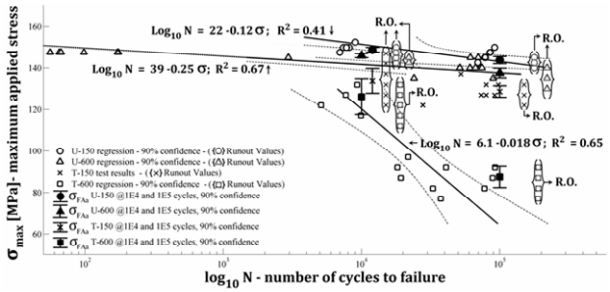

Fig. 11. S-N diagram relative to the U-150, U-600 and T-600 sets of FSW specimens with 90% confidence curves. Fatigue limits and run-out values – identified by { } R.O. marks – are sometimes shifted from the nominal 10^4 or 10^5 values for better readability.

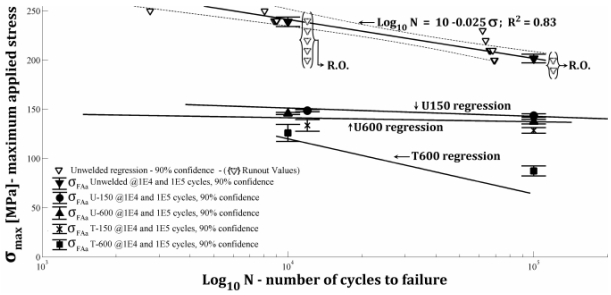

Fig. 12. Applied stress vs. number of cycles to failure diagram of the unwelded and the FS-welded samples.

3.3 Fatigue behaviour

Figs. 11 and 12 report the results of the fatigue tests on both the FSW and the unwelded samples, as well as the average fatigue limits obtained from the staircase method and the linear regression of the S-N diagram. Aluminum alloys do not have a defined fatigue limit [51]: for this reason we decided to do tests at 10^4 and 10^5 load cycles and, with an appropriate statistical analysis (according to international standards) it was possible to forecast the trend of the fatigue resistance of this alloy for a number of cycles varying between 10^3 and 10^6 (90% confidence). The fatigue limits at 10^4 load cycles of the unwelded, U-150, U-600, T-150 and T-600 samples were, respectively, equal to 239 ± 5 MPa, 149 ± 1 MPa, 146 ± 1 MPa, 134 ± 6 MPa and 126 ± 9 MPa. The fatigue limits at 10^5

Table 4. Fatigue tests results with an upper limit of 10,000 load cycles.

	U-150	U-600	T-150	T-600	BM
$\sigma_{FAa,10^4}$ (MPa)	148.8	145.9	133.8	126.2	239.0
μ (MPa)	1.5	13	12.8	18.2	5.3
$\hat{\mu}$ (MPa)	0.7	0.6	3.6	5.3	2.9
NR = Value not recorded					

Table 5. Fatigue tests results with an upper limit of 100000 load cycles.

	U-150	U-600	T-150	T-600	BM
$\sigma_{FAa,10^5}$ (MPa)	143.8	137.5	128.7	87.5	201.7
μ (MPa)	2.1	2.9	4.1	8.7	5.3
$\hat{\mu}$ (MPa)	1.1	1.4	1.7	3.1	2.7
NR = value not recorded					

load cycles were, in the same order, equal to: 202 ± 4 MPa, 144 ± 2 MPa, 138 ± 2 MPa, 129 ± 3 MPa and 88 ± 5 MPa.

The mean and the population standard deviation, as well as the sample standard deviation, were reconstructed from the staircase data, following the procedure reported in Ref. [46], and reported in Tables 4 and 5. A 90% confidence interval (k90% = 1.645) was adopted from the normal distribution to determine the scatter around fatigue limits, defined as and presented in the aforementioned values as well as in Figs. 9 and 10. A maximum scatter of 9 MPa was found for the threaded tool welded samples, for the 104 load cycles fatigue limit. Furthermore, a relatively low data dispersion resulted, even if the U-150 series presented only 10 specimens, instead of 15: the maximum scatter relative to this series resulted to be slightly inferior to 2 MPa.

By looking at Figs. 11 and 12, it is possible to state that the series of samples welded with the lower feed rate of 150 mm/min and the unthreaded tool exhibited the best fatigue behavior. Inferior fatigue strength was shown, from the best to the worst, by the U-600, T-150 and T-600 samples. Compared with the fatigue limits of the U-150 samples, a drop of, respectively, 2 %, 10% and 15% at 10^4 load cycles and of 4%, 11% and 39% at 10^5 load cycles resulted.

Therefore, the use of the threaded tool produced worse results than those obtained with the unthreaded one and the performances of the joints welded with the latter were only slightly influenced by the feed rates, as shown by the limited decrease in the fatigue resistance that followed by using a feed rate of 600 mm/min instead of 150 mm/min on an unthreaded tool. In fact, even if the relatively large standard deviations related to the threaded measurements at the 10^4 fatigue life limit do not allow to have full confidence in the results, the lower fatigue strength of the T-150 and T-600 series at the 10^5 limit, showing, respectively, a 11% and a 39% drop if compared to the U-150 samples, with relatively limited data dispersion, clarifies unambiguously that the performance of the joints obtained with the threaded tool was worse.

As a matter of fact, the use of the present threaded tool is more sensitive to the feed rate increase and would require an accurate selection of optimized values of this parameter.

The fatigue life S-N diagrams of the FS-welded specimens are presented in Fig. 11, and they have been obtained from the least squares linear regression procedure presented in ASTM E 739–91 standard [49], using as the independent variable X and $\log_{10}$ N as the dependent variable Y. A least squares linear regression fit of the form:

$$\boldsymbol{log_{10}N = A + B\sigma,} \tag{1}$$

has been adopted, estimating A and B coefficients by minimizing the squared distance from the measured points:

$$\boldsymbol{\hat{B} = \frac{\sum_{i=1}^{k}(X_i-\bar{X})*(Y_i-\bar{Y})}{\sum_{i-1}^{k}(X_i-\bar{X})^2},} \tag{2}$$

$$\boldsymbol{\hat{A} = \bar{Y} - \hat{B}\bar{X},} \tag{3}$$

where $Y = \log_{10} N$ and $X = \sigma$, k being the number of samples. The sample estimate of the variance is defined as:

$$\boldsymbol{\bar{\sigma}^2 = \frac{\sum_{i=1}^{k}(Y_i-\bar{Y}_i)}{\sum_{i=1}^{k}(K-Z)},} \tag{4}$$

where $\hat{Y}_i = \hat{A} + \hat{B}X_i$. The 90% hyperbolic confidence bands can be then obtained from the equation:

$$\boldsymbol{Y_{c,90\%} = \hat{A} + \hat{B}X \pm \sqrt{2F_{90\%}}\,\bar{\sigma}\,\sqrt{\left[\frac{1}{k} + \frac{(X-\bar{X})^2}{\sum_{i=1}^{k}(X_i-\bar{X})^2}\right]},} \tag{5}$$

where F90% is the F-test parameter for 90% confidence, with degrees of freedom $n_1 = 2$ and $n_2 = k-2$, following the nomenclature of the ASTM standard. Values for the regression analysis were taken from experimental data, remembering to exclude from the analysis the samples with not reported values of N, as well as run-out tests, according to the ASTM standard. The curve from the T-150 dataset is not presented since, due to the high number of run-outs at 10^4 cycles, which caused a low availability of samples, moreover concentrated only at N values around 10^5 cycles, it was not possible to extract a satisfactory trend, and the resulting determination coefficient R_2 was excessively low, with a value of 0.13.

Fig. 12 presents a comparison of the welded specimens S-N curves with the unwelded specimens BM series S-N curve, obtained with the same methodology. The superior fatigue behavior of the unwelded material is quite clear. In fact, a drop of 38% and 29% was experienced by the best welded samples, i.e. the U-150 ones, with an upper limit of, respectively, 10^4 and 10^5 load cycles. However, it is interesting to note that, for the unthreaded series, the reduction of fatigue strength is limited at the higher number of cycles since the gradient of the S-

Table 6. Tensile and fatigue strength efficiency and rate of fatigue strength decay of the samples.

Series ID	Tensile strength efficiency	Fatigue strength	
		10^4 LC	10^5 LC
BM	-	-	-
U-150	62%	62%	71%
U-600	59%	61%	68%
T-150	62%	56%	64%
T-600	59%	53%	43%

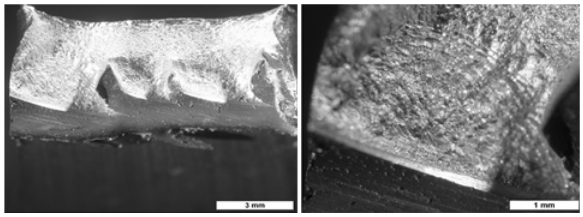

(a) (b)

Fig. 13. Fracture surface of specimens: (a) 10^4 cycles failure; (b) 10^5 cycles failure.

N curves of the unthreaded series of the welded samples is less steep than that of the unwelded ones. Therefore, the decay of the fatigue properties after the FSW process tends to become less important as the reference number of load cycles increases, at least if we are considering the samples welded with the unthreaded tool.

On the other hand, the T-600 series shows the same slope, i.e., exponent of Wöhler's diagram or decay rate of the BM. T-600 has an exponent $\log(\sigma_{10}^{5})$-$\log(\sigma_{10}^{4})$ that is close to those reported in the Eurocode 9 for some structural details. In the case of U-series, the values are close to tensile strength, hence there must have been a very high cyclic plastic strain, which can produce dynamic recrystallization ending up in dislocation cells, altering microstructure.

Some analyses were carried out on the broken samples. The images reported in Fig. 13 show the detail of a cracking surface of a specimen tested at 10^4 and 10^5 cycles, respectively. All the fatigue cracks are localized outside of the joint line, in the heat affected zone. In the case of specimens broken at 10^4 cycles, the fracture surface is rough and wrinkled (Fig. 13(a)). On the opposite, the specimens broken at 10^5 cycles (Fig. 13(b)) show a clear separation between the area of stable defect propagation and the area subjected to the final rupture. The beach marks, typical of the fatigue crack region, can be noticed in the area characterized by a smooth and bright surface.

Table 6 reports both the tensile and the fatigue efficiencies of the tested joints with respect to the strength of the base material. Efficiencies between 71% and 43% were found at the fatigue life limit of 10^5 load cycles. This means that the FS-welded AA6060-T6 alloy showed an efficiency drop of only 3%, from 71% to 68%, by increasing the feed rate by 400%, i.e., from 150 mm/min to 600 mm/min, and using the unthreaded tool. Furthermore, apart from when the higher feed rate was used, the efficiency of 64% of the joints welded with the threaded tool is comparable with those of the U-series. Therefore, if the samples of the U-150, U-600 and T-150 series are taken into account, the variation of the feed rate and tool shape did not give rise to remarkably different results. Analogously, in Ref. [22] Cirello et al. found that the influence of the variation of the FSW process parameters on the fatigue behavior of AA6082-T6 butt joints was quite low. The investigated feed rate range was between 71 and 215 mm/min, which falls around the lower speed value used in the present study, and the efficiency of the joints at the best condition was 60%. Compared with these results, those of the present study can be significant, particularly if the trend of the fatigue resistance of the best three series of the welded joints analyzed was confirmed at fatigue lives longer than 10^5 cycles. Furthermore, it is important to stress that, at least with the adopted process parameters, no beneficial effects on the fatigue strength can be obtained if a threaded tri-flute tool is used instead of a cylindrical standard one. Even though the adopted parameters are in line with the literature, the rotational speed was kept constant in this study and only the effect of feed rate was investigated. It is not possible to exclude different effects in terms of fatigue strength due to the use of other values of rotational speed.

The effect of the variation of the feed rate within a very similar range to that of interest on the LCF behavior of 6061Al-T651 friction stir welded joints was studied by Feng et al. in Ref. [10]. Despite the different fatigue regime accounted for, it is worth underlining that they found the fatigue lifetime to slightly decrease with increasing welding speed from 200 mm/min to 600 mm/min, that is, from a macroscopic point of view, coherent with what has been observed in the present AA6060-T6 joints. As far as the high cycle fatigue regime is concerned, the results collected meet those by Kim et al. [11], who observed that the fatigue resistance, with an upper limit of $2 \cdot 10^6$ cycles, of FS-welded joints of A6005-T5 extruded aluminum alloy sheets decreased with the increase of feed rate from 300 mm/min to 650 mm/min.

Furthermore, by comparing the micrographic analyses (Fig. 10) and the fatigue results, the fatigue samples failed in the heat affected zone, where the grain size is larger. As expected, the samples series having the largest grain dimension (T-600) showed the worst fatigue behavior.

4. Conclusions

The tensile and fatigue behavior of AA6060-T6 friction stir welded butt joints was investigated in this work. Micrographic and microhardness analyses across the joint region were also carried out. Generally good results in terms of welding efficiency were observed in almost all cases. Feed rate resulted to be a parameter affecting the UTS; in particular, the UTS increased for decreasing values of the feed rate. The tool geometry only influenced the strain at rupture and the threaded tool resulted in being detrimental to the strain limit. The width of the softened region and the microhardness values recorded in

the joining area resulted in being influenced by the feed rate; in particular, the width of the softened area increased with decreasing values of this parameter. In this case, the thermal contribution can be considered as the most significant factor affecting the softening effect: the higher the thermal contribution, the wider the softening width. As a general remark, the average grain size in the nugget area is always smaller when the threaded tool is used, thereby confirming a higher remixing effect due to its complex shape. Considering the HAZ, a certain correlation between the mechanical properties of the joints and the grain size can be observed: the average grain size of the retreating side, where the failure occurred, is usually larger than the advancing one. With regards to the joints fatigue properties, the samples welded with the lower feed rate and the unthreaded tool exhibited the best fatigue behavior. The use of the threaded tool gave rise to worst results, particularly at the higher feed rate and at the longer fatigue life. Furthermore, the performance of the joints welded with the standard tool was only slightly influenced by the feed rate.

Acknowledgments

The authors wish to thank Dr. Francesco Villa for the help in the execution of the fatigue data statistical analysis and representation, and for the general article revision.

Nomenclature

N	: Number of load cycles to failure
$\sigma_{\max}$	: Maximum applied stress over the fatigue cycle (MPa)
$\sigma_{FAa,10^4}$	: Mean value of fatigue limit at 10^4 load cycles (MPa)
$\sigma_{FAa,10^5}$	: Mean value of fatigue limit at 10^5 load cycles (MPa)
$\{\ \}R.O.$	: Run-out value, not included in linear regression, used with the staircase method
μ	: Population standard deviation of the fatigue limit (MPa)
$\hat{\mu}$	: Sample mean standard deviation of the average fatigue limit (MPa)
$\bar{Y}$	: Mean value of the Y variable
$\hat{Y}$	: Estimated value of the Y variable
Y_i	: i-th measure of the Y variable
$k_{90\%}$	: 90% confidence factor
S	: Tool rotational speed (rpm)
F	: Feed rate (mm/min)

References

[1] W. M. Thomas, E. D. Nichola, J. C. Needam, M. G. Murch, P. Templesmith and C. J. Dawes, *GB Patent Application No. 9125978-8* (1991).

[2] W. M. Thomas, E. D. Nichola, J. C. Needam, M. G. Murch, P. Templesmith and C. J. Dawes, *US Patent Application No. 5460317.P.L* (1995).

[3] R. Nandan, T. DebRoy and H. K.D.H. Bhadeshia, Recent advances in friction-stir welding - Process, weldment structure and properties, *Prog. Mater. Sci*., 53 (2008) 980–1023.

[4] S. Lomolino, R. Tovo andJ. dos Santos, On the fatigue behaviour and design curves of friction stir butt-welded Al alloys, *Int. J. Fatigue*, 27 (2005) 305–316.

[5] M. Grujicic, G. Arakere, B. Pandurangan, A. Hariharan, C.-F. Yen, B. A. Cheeseman and C. Fountzoulas, Statistical analysis of high-cycle fatigue behavior of friction stir welded AA5083-H321, *J. Mater. Eng. Perform*., 20 (2011) 855–864.

[6] A. Pirondi and L. Collini. Analysis of crack propagation resistance of Al–Al2O3 particulate-reinforcedcomposite friction stir welded butt joints, *International Journal of Fatigue*, 31 (2009) 111–121.

[7] L. Ceschini, I. Boromei, G. Minak, A. Morri and F. Tarterini. Effect of friction stir welding on microstructure, tensile and fatigue properties of the AA7005/10 vol.%Al2O3p composite, *Compos Sci Technol*, 67(3-4) (2007) 605–15.

[8] A. S. Franchim, F. F. Fernandez and D. N. Travessa, Microstructural aspects and mechanical properties of friction stir welded AA2024-T3 aluminium alloy sheet, *Mater. Des*., 32 (2011) 4684–4688.

[9] S. Malarvizhi and V. Balasubramanian, Effect of welding processes on AA2219 aluminium alloy joint properties, *Trans. Nonferrous Met. Soc. China*, 21 (2011) 962–973.

[10] A. H. Feng, D. L. Chen and Z. Y. Ma, Microstructure and low-cycle fatigue of a friction-stir-welded 6061 aluminum alloy, *Metall. Mater. Trans*., A 41A (2010) 2626–2641.

[11] W.-K. Kim, S.-T. Won and B.-C. Goo, A study on mechanical characteristics of the friction stir welded A6005-T5 extrusion, *Int. J. Prec. Eng. Manuf*., 11 (2010) 931–936.

[12] P. M. G. P. Moreira, F. M. F. de Oliveira and P. M. S. T. de Castro, Fatigue behaviour of notched specimens of friction stir welded aluminium alloy 6063-T6, *J. Mater. Process. Technol*., 207 (2008) 283–292.

[13] P. M. G. P. Moreira, M. A. V. de Figueiredo and P. M. S. T. de Castro, Fatigue behaviour of FSW and MIG weldments for two aluminium alloys, *Theor. Appl. Fract. Mech*., 48 (2007) 169–177.

[14] T. Okada, M. Suzuki, H. Miyake, T. Nakamura, S. Machida and M. Asakawa, Evaluation of crack nucleation site and mechanical properties for friction stir welded butt joint in 2024-T3 aluminum alloy, *Int. J. Adv. Manuf. Technol*., 50 (2010) 127–135.

[15] G. Campanile, A. Prisco, A. Squillace, C. Bitondo, G. Dionoro, P. Buonadonna, A. Tronci, L. Fratini and D. Palmeri, FSW of AA2139-T8 Butt joints for aeronautical applications, *Proc. Inst. Mech. Eng. Pt. L-J. Mater.-Design Appl.*, 225 (2011) 87–101.

[16] M. Aissani, S. Gachi, F. Boubenider and Y. Benkedda, Design and optimization of friction stir welding tool, *Mater. Manuf. Process*., 25 (2010) 1199–1205.

[17] H. Aydin, A. Bayram, U. Esme, Y. Kazancoglu and O. Guven, Application of grey relation analysis (GRA) and

Taguchi method for the parametric optimization of friction stir welding (FSW) process, *Mater. Tehnol*., 44 (2010) 205–211.

[18] D. M. Rodrigues, A. Loureiro, C. Leitao, R. M. Leal, B. M. Chaparro and P. Vilaça, Influence of friction stir welding parameters on the microstructural and mechanical properties of AA 6016-T4 thin welds, *Mater. Des*., 30 (2009) 1913–1921.

[19] H. Lombard, D. G. Hattingh, A. Steuwer and M. N. James, Optimising FSW process parameters to minimise defects and maximise fatigue life in 5083-H321 aluminium alloy, *Eng. Fract. Mech*., 75 (2008) 341–354.

[20] D. G. Hattingh, C. Blignault, T. I. van Niekerk and M. N. James, Characterization of the influences of FSW tool geometry on welding forces and weld tensile strength using an instrumented tool, *J. Mater. Process. Technol*., 203 (2008) 46–57.

[21] K. Kumar, S. V. Kailas and T. S. Srivatsan, Influence of tool geometry in friction stir welding, *Mater. Manuf. Process*., 23 (2008) 189–195.

[22] A. Cirello, G. Buffa, L. Fratini and S. Pasta, AA6082-T6 friction stir welded joints fatigue resistance: influence of process parameters, *Proc. Inst. Mech. Eng. Part B-J. Eng. Manuf*., 220 (2006) 805–811.

[23] O. Hatamleh, I. V. Rivero and S. E. Swain, An investigation of the residual stress characterization and relaxation in peened friction stir welded aluminum–lithium alloy joints, *Mater. Des*., 30 (2009) 3367–3373.

[24] O. Hatamleh, Effects of peening on mechanical properties in friction stir welded 2195 aluminum alloy joints, *Mater. Sci. Eng. A-Struct. Mater. Prop. Microstruct. Process*., 492 (2008) 168–176.

[25] O. Hatamleh, I. V. Rivero and J. Lyons, Evaluation of surface residual stresses in friction stir welds due to laser and shot peening, *J. Mater. Eng. Perform*., 16 (2007) 549–553.

[26] L. Fratini and B. Zuccarello, An analysis of through-thickness residual stresses in aluminium FSW butt joints, *Int. J. Mach. Tools Manuf*., 46 (2006) 611–619.

[27] M. N. James, D. G. Hattingh, D. J. Hughes, L.-W. Wei, E. A. Patterson and J. Q. Da Fonseca, Synchrotron diffraction investigation of the distribution and influence of residual stresses in fatigue, *Fatigue Fract. Eng. Mater. Struct.*, 27 (2004) 609–622.

[28] S. Malarvizhi and V. Balasubramanian, Fatigue crack growth resistance of gas tungsten arc, electron beam and friction stir welded joints of AA2219 aluminium alloy, *Mater. Des*., 32 (2011) 1205–1214.

[29] O. Hatamleh, J. Lyons and R. Forman, Laser and shot peening effects on fatigue crack growth in friction stir welded 7075-T7351 aluminum alloy joints, *Int. J. Fatigue*, 29 (2007) 421–434.

[30] A.-L. Lafly, C. D. Donne, G. Biallas, D. Allehaux and F. Marie, Role of residual stresses on fatigue crack propagation of FSW 6056-T78 aluminium joints under various technologies, *Materials Science Forum*, 519–521 (2006) 1089–1094.

[31] S. Hong, S. Kim, C. G. Lee and S.-J. Kim, Fatigue crack propagation behavior of friction stir welded Al–Mg–Si alloy, *Scr. Mater.*, 55 (2006) 1007–1010.

[32] G. Bussu and P. E. Irving, The role of residual stress and heat affected zone properties on fatigue crack propagation in friction stir welded 2024-T351 aluminium joints, *Int. J. Fatigue*, 25 (2003) 77–88.

[33] L. Fratini, G. Macaluso and S. Pasta, Residual stresses and FCP prediction in FSW through a continuous FE model, *J. Mater. Process. Technol*., 209 (2009) 5465–5474.

[34] A. F. Golestaneh, A. Ali and M. Zadeh, Modelling the fatigue crack growth in friction stir welded joint of 2024-T351 Al alloy, *Mater. Des*., 30 (2009) 2928–2937.

[35] S. G. Pantelakis and N. D. Alexopoulos, Assessment of the ability of conventional and advanced wrought aluminum alloys for mechanical performance in light-weight applications, *Mater. Des*., 29 (2008) 80–91.

[36] O. Engler and J. Hirsch, Texture control by thermomechanical processing of AA6xxx Al–Mg–Si sheet alloys for automotive applications - a review, *Mater. Sci. Eng. A-Struct. Mater. Prop. Microstruct. Process*., 336 (2002) 249–262.

[37] W. S. Miller, L. Zhuang, J. Bottema, A. J. Wittebrood, P. De Smet, A. Haszler and A. Vieregge, Recent development in aluminium alloys for the automotive industry, *Mater. Sci. Eng. A-Struct. Mater. Prop. Microstruct. Process*., 280 (2000) 37–49.

[38] H. J. Aval, S. Serajzadeh and A. H. Kokabi, Evolution of microstructures and mechanical properties in similar and dissimilar friction stir welding of AA5086 and AA6061, *Mater. Sci. Eng. A-Struct. Mater. Prop. Microstruct. Process*., 528 (2011) 8071–8083.

[39] C. Gallais, A. Denquin, Y. Brechet and G. Lapasset, Precipitation microstructures in an AA6056 aluminium alloy after friction stir welding: Characterisation and modelling, *Mater. Sci. Eng. A-Struct. Mater. Prop. Microstruct. Process*, 496 (2008) 77–89.

[40] Y. S. Sato, H. Kokawa, M. Enomoto and S. Jogan, Microstructural evolution of 6063 Aluminum during friction-stir welding, *Metall. Mater. Trans. A-Phys. Metall. Mater. Sci.*, 30 (1999) 2429–2437.

[41] S. Xu and X. Deng, A study of texture patterns in friction stir welds, *Acta Mater*., 56 (2008) 1326–1341.

[42] D. P. Field, T. W. Nelson, Y. Hovanski and K. V. Jata, Heterogeneity of crystallographic texture in friction stir welds of aluminum, *Metall. Mater. Trans. A-Phys. Metall. Mater. Sci*., 32 (2001) 2869–2877.

[43] P. M. G. P. Moreira, A. M. P. de Jesus, A. S. Ribeiro and P. M. S. T. de Castro, Fatigue crack growth in friction stir welds of 6082-T6 and 6061-T6 aluminium alloys: A comparison, *Theor. Appl. Fract. Mech*., 50 (2008) 81–91.

[44] A. K. Lakshminarayanan, V. Balasubramanian and K. Elangovan, Effect of welding processes on tensile properties of AA6061 aluminium alloy joints, *Int. J. Adv. Manuf. Technol*., 40 (2009) 286–296.

[45] W. J. Dixon and F. J. Massey Jr, *Introduction to statistical*

analysis, McGraw-Hill, New York (1983) 386–94.
[46] R. Pollak, A. Palazotto and T. Nicholas, A simulation-based investigation of the staircase method for fatigue strength testing, *Mech. Mater*., 38 (2006) 1170–1181.
[47] S.-K. Lin, Y.-L. Lee and M.-W. Lu, Evaluation of the staircase and the accelerated test methods for fatigue limit distributions, *Int. J. Fatigue*, 23 (2001) 75–83.
[48] J. A. Collins, *Failure of materials in mechanical design*, wiley and sons, New York (1981) 369-374.
[49] American Society for Testing and Materials, *ASTM E 739–91: Standard Practice for Statistical Analysis of Linear or Linearized Stress Life (S-N) and Strain Life (ε- N)* (1991).
[50] American Society for Testing and Materials, *ASTM E112-12: Standard Test Methods for Determining Average Grain Size* (2012).
[51] ASM HANDBOOK, *Vol. 19 "Fatigue and Fracture"*, ASM International, USA (1996).

Sergio Baragetti is Full Professor of Machine Design and Computational Mechanics at the University of Bergamo (Italy). He graduated in Mechanical Engineering from Politecnico di Milano. Ph.D. in Quality Engineering, Università di Firenze. He is the Director of GITT - Centre on Innovation Management and Technology Transfer and of the Structural Mechanics Lab of the University of Bergamo. Delegate of the Rector for NETVAL. His research activities include the study of effects induced by surface treatments on the fatigue behaviour of mechanical components, corrosion fatigue mechanisms in aqueous environments, surface thin hard coatings effects on fatigue, contact and corrosion fatigue.

Gianluca D'Urso is Assistant Professor at the Department of Engineering, University of Bergamo. He received his degree in Management Engineering at the University of Bergamo (Italy), Ph.D. in Manufacturing Engineering at the University of Padova (Italy). He is deputy director of GITT - Centre on Innovation Management and Technology Transfer. And he is member of AITEM, the Italian Association of Manufacturing Engineers. His main research activities include analysis of welding technologies based on FSW (Friction Stir Welding) by means of experimental and simulative (FEM) methods, experimental and FEM analysis of forming and machining processes, microfabrication technologies using micro-EDM (Electro Discharge Machining) and EBL (Electron Beam Lithography).